Eur. Phys. J. E (2013) **36**: 26
DOI 10.1140/epje/i2013-13026-y

THE EUROPEAN PHYSICAL JOURNAL E

Regular Article

On the moving contact line singularity: Asymptotics of a diffuse-interface model

David N. Sibley[1], Andreas Nold[1], Nikos Savva[2,1], and Serafim Kalliadasis[1,a]

[1] Department of Chemical Engineering, Imperial College London, London SW7 2AZ, UK
[2] School of Mathematics, Cardiff University, Senghennydd Road, Cardiff CF24 4AG, UK

Received 4 October 2012 and Received in final form 6 February 2013
Published online: 22 March 2013 –

Abstract. The behaviour of a solid-liquid-gas system near the three-phase contact line is considered using a diffuse-interface model with no-slip at the solid and where the fluid phase is specified by a continuous density field. Relaxation of the classical approach of a sharp liquid-gas interface and careful examination of the asymptotic behaviour as the contact line is approached is shown to resolve the stress and pressure singularities associated with the moving contact line problem. Various features of the model are scrutinised, alongside extensions to incorporate slip, finite-time relaxation of the chemical potential, or a precursor film at the wall.

1 Introduction

A moving contact line occurs at the location where two ostensibly immiscible fluids and a solid meet. It arises in a wide range of both natural and technological processes, from insects walking on water [1] and the wetting properties of plant leaves [2] to coating [3], inkjet printing [4, 5] and oil recovery [6]. In addition to its crucial role in wide-ranging applications, it remains a persistent problem, a long-standing and fundamental challenge in the field of fluid dynamics, despite its apparent simplicity at first sight (see *e.g.* review articles [7–10]). Not surprisingly it has been investigated extensively, both experimentally and theoretically, for several decades.

At the heart of the moving contact line problem is that, when treated classically as two immiscible fluids moving along a solid surface satisfying the no-slip condition, there is no solution due to the multivalued velocity at the contact line, [11,12]. This is known most famously in the literature as the problem of a non-integrable stress singularity, a result published a few decades ago along with the non-physical prediction that an infinite force is required to submerge a solid object [13].

The resolution of the problem may have initially appeared straightforward. The no-slip condition at the wall could not be satisfied, thus some form of slip in the contact line vicinity should be allowed. Navier-slip, written down in the early 19th Century [14], was a prime candidate, a form of which was suggested in the concluding remarks of [13]. The fact that wetting and the moving contact line remain an open debate and a fruitful research area is largely due to the particular microscale ingredients that may alleviate the problem being numerous and hotly debated—see *e.g.* the wide range of discussion articles recently, [15]. Various alternative models to slip at the wall include: a precursor film ahead of the contact line [16]; rheological effects [17]; treating surfaces as separate thermodynamic entities with dynamic surface tensions [18] (see a recent critical investigation of this model, [19]); introducing numerical slip [20]; including evaporative fluxes [21]; and considering the interface to be diffuse, numerical work reviewed *e.g.* in [22].

Here, we examine analytically a diffuse-interface model without any other ingredients, being both self-consistent and physically relevant: rather than considering a sharp fluid-fluid interface as a surface of zero thickness where quantities (*e.g.* density) are, in general, discontinuous, it considers the interface to have a non-zero, finite, thickness with quantities varying smoothly but rapidly, in agreement with developments from the statistical mechanics of liquids community (*e.g.* [23,24]). The fluid density $\bar{\rho}$ then acts as an order parameter such that in the sharp-interface limit the two bulk fluids satisfy $\bar{\rho} = \rho_L$ and $\bar{\rho} = \rho_V = 0$, being liquid and vapour, respectively, where we consider the behaviour of the system with vapour phase of negligible density, noting that an equivalent double-well free energy form (to be described later, in sect. 2), with zero bulk vapour density, is also used by Pismen and Pomeau [25] and is physically relevant for liquid-gas systems. The interface between liquid and gas may then be defined as the location where $\bar{\rho} = (\rho_L + \rho_V)/2$.

Diffuse-interface models have been popular for numerical implementation as tracking of the fluid-fluid interface is not required in the resulting free-boundary problem,

[a] e-mail: S.Kalliadasis@imperial.ac.uk

instead the interface is inferred from density field contours. For solid-liquid-gas systems the seminal study of Seppecher [26] is often referred to when suggesting that diffuse-interface models resolve the moving contact line problem. Whilst Seppecher's work contains some discussion of the asymptotics, the analysis was largely incomplete, with asymptotic regions being probed without careful justification and the crucial behaviour close to the contact line only investigated numerically (a number of constraints were also imposed, *e.g.* 90° contact angles and fluids of equal viscosity). Full numerical simulations for the liquid-gas problem have also been undertaken (*e.g.* in [27, 28]); binary fluids have also been examined using diffuse-interface methods of a different form, where a coupled Cahn-Hilliard equation models the diffusion between the two components [29–31].

Here, we undertake an analytical investigation by considering the contact line behaviour for a liquid-gas system with two basic elements: a) the interface has a finite thickness, which is expected from statistical mechanics studies as noted earlier, and b) the no-slip condition is applied at the wall. This diffuse-interface model then resolves the moving contact line problem without the need to model any further physical effects from the microscale. An important ramification of this analysis is that the wetting boundary condition used in conjunction with a diffuse-interface in existing numerical studies of liquid-gas systems needs to be appropriately modified, otherwise it leads to a density gradient orthogonal to the wall at large distances from the contact line. The possibility of density variations such as these are often included when disjoining pressure models are considered, where many studies utilise the long-wave (or lubrication) approximation, *e.g.* [8,32]. In the 1985 review of de Gennes [8], the thickness of precursor films was discussed. For complete wetting on a dry substrate, nanometric films, decaying ahead of the contact line, were predicted. A recent study of intermolecular forces in the contact line region using approaches from statistical mechanics, namely density-functional theory [33], demonstrated that for the case of partially wetting fluids, a constant-thickness nanometric film of a few molecular diameters is adsorbed in front of the contact line. More recent experiments have also been performed (*e.g.* to probe the dynamics of such nanoscale films [34]).

In the macro/mesoscopic setting of this work, and to isolate the contribution of the diffuse-interface model without depletion/enrichment near the solid substrate, we thus predominately consider the case where the bulk densities are valid up to the walls (but other cases are considered), and we make no assumptions on thin films—rather considering arbitrary finite contact angles.

2 Problem specification

Consider a fluid in the upper half $(\bar{x},\bar{y})$-plane Ω with a solid surface $\partial\Omega$ at $\bar{y}=0$; see fig. 1. The free energy of the system has contributions from an isothermal fluid with a Helmholtz free energy functional and from a wall energy

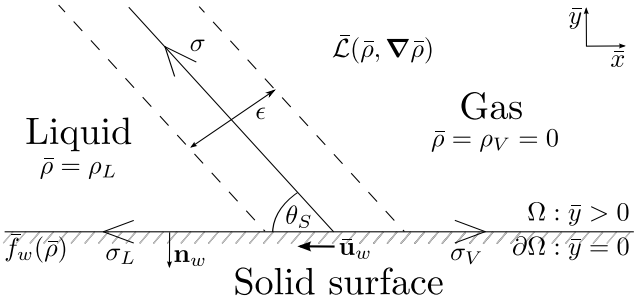

Fig. 1. Sketch of the diffuse-interface model near a wall.

$f_w = f_w(\bar{\rho})$, thus given by $\mathscr{F} = \int_\Omega \bar{\mathcal{L}}\,\mathrm{d}\Omega + \int_{\partial\Omega} f_w\,\mathrm{d}A$, where

$$\bar{\mathcal{L}} = \bar{\rho}\bar{f}(\bar{\rho}) + K|\boldsymbol{\nabla}\bar{\rho}|^2/2 - \bar{G}\bar{\rho}, \tag{1}$$

with $\bar{G}$ the chemical potential, K a gradient energy coefficient (assumed constant for simplicity), and $\bar{\rho}\bar{f}(\bar{\rho})$ a double well potential chosen to give the two equilibrium states $\bar{\rho}=\{0,\rho_L\}$. Such a form for the free energy and associated diffuse-interface approximations has been used by numerous authors for wetting problems such as Seppecher [26], Pismen and Pomeau [25], and Pismen [35]; see also the review by de Gennes [8]. The effect of the non-local terms neglected in the local approximation to obtain such a free energy has been considered at equilibrium in the aforementioned studies [35,33], where the long-range intermolecular interactions are responsible for an algebraic decay of the density profile away from the interface instead of the exponential one as predicted here (seen later, in (10)). In our dynamic situation, we focus on the local approximation to elucidate the contact line behaviour in a simplified, yet widely used setting. The density field augments the usual hydrodynamic equations via the capillary (or Korteweg) stress tensor $\bar{\mathsf{T}}$ through

$$\bar{f}(\bar{\rho}) = \frac{K}{2\epsilon^2}\bar{\rho}\left[1-\frac{\bar{\rho}}{\rho_L}\right]^2, \quad \bar{\mathsf{T}} = \bar{\mathcal{L}}\mathsf{I} - \boldsymbol{\nabla}\bar{\rho}\otimes\frac{\partial\bar{\mathcal{L}}}{\partial(\boldsymbol{\nabla}\bar{\rho})}, \tag{2}$$

where I is the identity tensor, and with ϵ being the interface width, and $\bar{\mathsf{T}}$ arising from Noether's theorem, [22]. Following [26], [22] and [25], using (1) and coupling in the compressible Stokes equations (assuming creeping flow) the capillary tensor with the usual viscous stress tensor $\bar{\boldsymbol{\tau}}$, taken as deviatoric for simplicity, yields

$$\begin{gathered}
\partial_{\bar{t}}\bar{\rho} + \boldsymbol{\nabla}\cdot(\bar{\rho}\bar{\mathbf{u}}) = 0, \qquad \boldsymbol{\nabla}\cdot(\bar{\mathsf{T}}+\bar{\boldsymbol{\tau}}) = 0,\\
\bar{\mathsf{T}} = \left(\bar{\rho}\bar{f}(\bar{\rho}) + K|\boldsymbol{\nabla}\bar{\rho}|^2/2 - \bar{G}\bar{\rho}\right)\mathsf{I} - K\boldsymbol{\nabla}\bar{\rho}\otimes\boldsymbol{\nabla}\bar{\rho},\\
\bar{\boldsymbol{\tau}} = \bar{\mu}(\bar{\rho})\left[(\boldsymbol{\nabla}\bar{\mathbf{u}}) + (\boldsymbol{\nabla}\bar{\mathbf{u}})^{\mathrm{T}} - 2(\boldsymbol{\nabla}\cdot\bar{\mathbf{u}})\mathsf{I}/3\right],\\
\bar{G} = -K\nabla^2\bar{\rho} + \partial_{\bar{\rho}}(\bar{\rho}\bar{f}(\bar{\rho})),
\end{gathered} \tag{3}$$

where $\bar{\mathbf{u}}$ and $\bar{\mu}(\bar{\rho})$ are the fluid velocity and viscosity, respectively, $\bar{t}$ is time, and the thermodynamic pressure is given by $\bar{p} = \bar{\rho}^2\bar{f}'(\bar{\rho})$. The form for $\bar{G}$ arises from the Euler-Lagrange equation corresponding to the free energy, and we take $\bar{\mu}(\bar{\rho}) = \mu_L\bar{\rho}/\rho_L$, giving the viscosities for the two equilibrium states as μ_L and $\mu_V = 0$.

On the solid surface $\partial\Omega$, with normal $\mathbf{n}_w$, we impose

$$\bar{\mathbf{u}} = \bar{\mathbf{u}}_w, \qquad K\mathbf{n}_w\cdot\boldsymbol{\nabla}\bar{\rho} + \bar{f}_w'(\bar{\rho}) = 0, \tag{4}$$

with wall velocity $\bar{\mathbf{u}}_w = (-V, 0)$ in Cartesian coordinates. The first condition is classical no-slip, whilst the second arises by variational arguments and is termed the *natural* (or *wetting*) boundary condition, [36]. $\bar{f}_w(\bar{\rho})$ is chosen to satisfy Young's law at the contact line, with solid-liquid, solid-gas and liquid-gas surface tensions $\bar{f}_w(\rho_L) = \sigma_L$, $\bar{f}_w(\rho_V) = \sigma_V$ and σ, respectively, and with contact angle θ_S. A cubic is the lowest-order polynomial required for the wall free energy to be minimised by the bulk densities, to prevent depletion/enrichment away from the contact line, *i.e.* $\bar{f}'_w(\bar{\rho}_L) = \bar{f}'_w(0) = 0$. Whilst cubic forms are used for binary fluid problems, *e.g.* [37,31], this is unlike the linear forms proposed in previous studies for liquid-gas problems [26–28,38], and allows us to consider a diffuse-interface model without further physical effects from the microscale (although this is relaxed in the following section). We define

$$\bar{f}_w(\bar{\rho}) = \left[\rho_L^{-3}\sigma\cos\theta_S(4\bar{\rho}^3 - 6\bar{\rho}^2\rho_L + \rho_L^3) + \sigma_V + \sigma_L\right]/2,$$

giving

$$\bar{f}'_w(\bar{\rho}) = -6\sigma\bar{\rho}\,(\rho_L - \bar{\rho})\cos\theta_S/\rho_L^3,$$

and $\bar{f}_w(0) - \bar{f}_w(\rho_L) = \sigma\cos\theta_S$, with Young's law thus satisfied. It is noteworthy that (4)(b) may be replaced by a constant density condition if a precursor film/disjoining pressure model is to be considered, *i.e.* $\bar{\rho} = \rho_a$ on $\partial\Omega$ (as used in [25], and considered in the following section). Finally, for a one-dimensional density profile $\bar{\rho}(z)$ in equilibrium (*i.e.* with $\bar{G} = 0$ required by our choice of $\bar{\rho}\bar{f}(\bar{\rho})$ to have equally stable bulk fluids, and $\bar{\mathbf{u}} = 0$), the surface tension across the interface is

$$\sigma = K\int_{-\infty}^{\infty}\left(\frac{\mathrm{d}\bar{\rho}}{\mathrm{d}\bar{z}}\right)^2\mathrm{d}\bar{z} = \frac{K\bar{\rho}_L^2}{6\epsilon}\,, \tag{5}$$

see *e.g.* [39], and we note eqs. (3)–(4), without the specific choices for $\bar{\mu}(\bar{\rho})$, $\bar{f}(\bar{\rho})$ and $\bar{f}_w(\bar{\rho})$ are as derived/used in [26, 22,25]. To non-dimensionalise, we use typical length, velocity and density scales X, V and ρ_L, respectively. The pressure and viscous stress are scaled with $\mu_L V/X$, and the capillary stress with $K\rho_L^2/(\epsilon X)$. Finally, $\bar{G}$ is scaled with $K\rho_L/(\epsilon X)$ and $\bar{f}$ with $K\rho_L/\epsilon^2$. The governing equations then contain the non-dimensional parameters

$$\mathrm{Cn} = \epsilon/X, \quad \text{and} \quad \mathrm{Ca}_k = \mu_L V\epsilon/(K\rho_L^2),$$

being the Cahn number and a modified Capillary number based on the model parameter K, respectively. Non-dimensional variables are denoted as their dimensional counterparts with bars dropped, *e.g.* non-dimensional bulk densities are $\rho = \{0, 1\}$. Ca_k is related to the usual Capillary number, $\mathrm{Ca} = \mu_L V/\sigma = 6\,\mathrm{Ca}_k$, through (5). The governing equations (3) in non-dimensional form are

$$\begin{aligned}
&\partial_t\rho + \boldsymbol{\nabla}\cdot(\rho\mathbf{u}) = 0, \quad \mathsf{M} = \mathrm{Ca}_k{}^{-1}\mathsf{T} + \boldsymbol{\tau}, \quad \boldsymbol{\nabla}\cdot\mathsf{M} = 0,\\
&\mathsf{T} = \left(\mathrm{Cn}^{-1}\rho f(\rho) + \mathrm{Cn}|\boldsymbol{\nabla}\rho|^2/2 - G\rho\right)\mathsf{I} - \mathrm{Cn}\,\boldsymbol{\nabla}\rho\otimes\boldsymbol{\nabla}\rho,\\
&\boldsymbol{\tau} = \rho\left[(\boldsymbol{\nabla}\mathbf{u}) + (\boldsymbol{\nabla}\mathbf{u})^{\mathrm{T}} - 2(\boldsymbol{\nabla}\cdot\mathbf{u})\mathsf{I}/3\right],\\
&G = -\,\mathrm{Cn}\,\nabla^2\rho + \mathrm{Cn}^{-1}\partial_\rho(\rho f(\rho)),
\end{aligned} \tag{6}$$

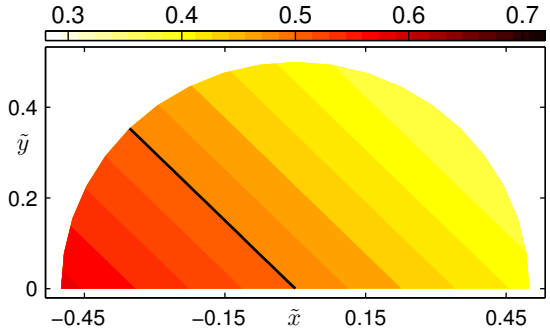

Fig. 2. The equilibrium density behaviour (contours) near the contact line for $\theta_S = \pi/4$, from eq. (10) in inner variables.

where M is introduced as the total stress tensor, $p = (\mathrm{Cn}\,\mathrm{Ca}_k)^{-1}\rho^2 f'(\rho)$, and from (2):

$$f(\rho) = \frac{\rho}{2}(1-\rho)^2, \quad \text{giving} \quad p = \frac{\rho^2(1-3\rho)(1-\rho)}{2\,\mathrm{Cn}\,\mathrm{Ca}_k}\,. \tag{7}$$

On the solid surface $\partial\Omega$, from (4), we have

$$\mathbf{u} = \mathbf{u}_w, \qquad \mathrm{Cn}\,\mathbf{n}_w\cdot\boldsymbol{\nabla}\rho = \cos\theta_S(1-\rho)\rho, \tag{8}$$

where $\mathbf{u}_w = (-1, 0)$, and $\mathbf{n}_w = (0, -1)$, in Cartesian components. We can rewrite the governing equations (6) for steady flows as

$$\begin{aligned}
&\boldsymbol{\nabla}\cdot(\rho\mathbf{u}) = 0,\\
&\boldsymbol{\nabla}p = (2\,\mathrm{Cn}\,\mathrm{Ca}_k)^{-1}\boldsymbol{\nabla}[\rho^2(1-3\rho)(1-\rho)],\\
&0 = \mathrm{Ca}_k^{-1}\,\mathrm{Cn}\,\rho\boldsymbol{\nabla}(\nabla^2\rho) - \boldsymbol{\nabla}p\\
&\quad + \rho[\boldsymbol{\nabla}^2\mathbf{u} + \boldsymbol{\nabla}(\boldsymbol{\nabla}\cdot\mathbf{u})/3]\\
&\quad + [(\boldsymbol{\nabla}\mathbf{u}) + (\boldsymbol{\nabla}\mathbf{u})^{\mathrm{T}} - 2(\boldsymbol{\nabla}\cdot\mathbf{u})\mathsf{I}/3]\boldsymbol{\nabla}\rho,
\end{aligned} \tag{9}$$

and the boundary conditions on $\partial\Omega$ remain as above, in (8). We initially consider the equilibrium behaviour of the system, corresponding to $\mathrm{Ca}_k \ll 1$, to provide a basis for comparison when the dynamic behaviour is analysed, where eqs. (8)–(9) are thus reduced to

$$2\mathrm{Cn}^2\rho\boldsymbol{\nabla}(\nabla^2\rho) = \boldsymbol{\nabla}\left[\rho^2(1-3\rho)(1-\rho)\right],$$

subject to $-\,\mathrm{Cn}\,\partial_y\rho = \cos\theta_S(1-\rho)\rho$ at $y = 0$, and with $\rho \to \{0, 1\}$ and $\nabla^2\rho \to 0$ as $x \to \pm\infty$ to obtain the expected bulk behaviour. The solution subject to the above conditions is

$$\rho = \left(1 - \tanh\left[(2\,\mathrm{Cn})^{-1}(x\sin\theta_S + y\cos\theta_S)\right]\right)/2, \tag{10}$$

having also fixed the interface at $\rho = 1/2$. This profile is planar and at angle θ_S, shown in fig. 2 in inner variables (where $\{x, y\} = \mathrm{Cn}\{\tilde{x}, \tilde{y}\}$, for comparison to forthcoming plots).

For physical systems, the scale over which the density varies between liquid and gas is much smaller than the macroscopic length scale, and hence $\mathrm{Cn} \ll 1$. The asymptotic behaviour as $\mathrm{Cn} \to 0$ is known as the sharp-interface limit, and understanding of it is of vital importance when

considering diffuse-interface models as classical continuum models should be recovered if correct predictions are to be found.

A careful asymptotic analysis of the outer solution away from the interface, and of the interfacial region away from the wall (using body fitted coordinates), shows that the expected sharp-interface equations (the Stokes equations with no-slip and the usual capillary surface stress conditions) are indeed recovered.

Consider now the inner region near to both interface and wall in polar coordinates with $r = O(\mathrm{Cn})$. The scaling $\boldsymbol{\nabla} = \mathrm{Cn}^{-1}\,\tilde{\boldsymbol{\nabla}}$ (*i.e.* $r = \mathrm{Cn}\,\tilde{r}$, with inner variables denoted with tildes) retains all terms in the governing equations and boundary conditions (8)–(9), giving a complete dominant balance. The steady governing equations, from (9), in this inner region are thus

$$\tilde{\boldsymbol{\nabla}} \cdot (\tilde{\rho}\tilde{\mathbf{u}}) = 0, \tag{11}$$

and

$$\begin{aligned}\mathrm{Ca}_k^{-1}\,\tilde{\rho}\tilde{\boldsymbol{\nabla}}(\tilde{\nabla}^2\tilde{\rho}) - (2\,\mathrm{Ca}_k)^{-1}\tilde{\boldsymbol{\nabla}}[\tilde{\rho}^2(1-3\tilde{\rho})(1-\tilde{\rho})] \\ + \tilde{\rho}[\tilde{\boldsymbol{\nabla}}^2\tilde{\mathbf{u}} + \tilde{\boldsymbol{\nabla}}(\tilde{\boldsymbol{\nabla}}\cdot\tilde{\mathbf{u}})/3] \\ + [(\tilde{\boldsymbol{\nabla}}\tilde{\mathbf{u}}) + (\tilde{\boldsymbol{\nabla}}\tilde{\mathbf{u}})^{\mathrm{T}} - 2(\tilde{\boldsymbol{\nabla}}\cdot\tilde{\mathbf{u}})\mathsf{I}/3]\tilde{\boldsymbol{\nabla}}\tilde{\rho} = 0,\end{aligned} \tag{12}$$

and on the solid surface $\partial\Omega$, the boundary conditions are

$$\tilde{\mathbf{u}} = \tilde{\mathbf{u}}_w, \qquad \mathbf{n}_w \cdot \tilde{\boldsymbol{\nabla}}\tilde{\rho} = \cos\theta_S(1-\tilde{\rho})\tilde{\rho}, \tag{13}$$

where in polar coordinates, and with $\tilde{u}$ and $\tilde{v}$ being the radial and angular velocity components, these reduce to

$$\tilde{u} = -1, \qquad \tilde{v} = 0, \qquad -\frac{1}{\tilde{r}}\frac{\partial\tilde{\rho}}{\partial\theta} = \cos\theta_S(1-\tilde{\rho})\tilde{\rho}, \tag{14}$$

on $\theta = 0$, and

$$\tilde{u} = 1, \qquad \tilde{v} = 0, \qquad \frac{1}{\tilde{r}}\frac{\partial\tilde{\rho}}{\partial\theta} = \cos\theta_S(1-\tilde{\rho})\tilde{\rho}, \tag{15}$$

on $\theta = \pi$. Of particular interest is the behaviour as the contact line is approached—the location where a stress singularity or no solution (due to multivalued velocity) arises in the classical formulation of the problem. To consider the asymptotic solution as the contact line is approached, we expand

$$\{\tilde{\rho}, \tilde{u}, \tilde{v}\} = \sum_{i=0}^{\infty}\{\tilde{\rho}_i(\theta), \tilde{u}_i(\theta), \tilde{v}_i(\theta)\}\,\tilde{r}^i,$$

in (11)–(12), and find at leading order

$$\tilde{\rho}_0(\tilde{u}_0 + \tilde{v}_0') = -\tilde{\rho}_0'\tilde{v}_0, \qquad \tilde{\rho}_0''' = 0, \qquad \tilde{\rho}_0'' = 0,$$

subject to $\tilde{\rho}_0' = 0$ on $\theta = \{0, \pi\}$, from (14)–(15). The density is solved as $\tilde{\rho}_0 = 1/2$, having imposed its expected value at the interface. To find the leading-order velocities, we continue to first order in the governing equations (11)–(12), where

$$\begin{gathered}\tilde{u}_0 = -\tilde{v}_0', \qquad \mathrm{Ca}_k(\tilde{v}_0''' + \tilde{v}_0') + \tilde{\rho}_1'' + \tilde{\rho}_1 = 0, \\ \mathrm{Ca}_k(\tilde{v}_0'' + \tilde{v}_0) - \tilde{\rho}_1''' - \tilde{\rho}_1' = 0.\end{gathered}$$

with the wetting and no-slip conditions from (14)–(15) being

$$\tilde{u}_0 = -1, \qquad \tilde{v}_0 = 0, \qquad -\tilde{\rho}_1' = \cos(\theta_S)/4,$$

on $\theta = 0$, and

$$\tilde{u}_0 = 1, \qquad \tilde{v}_0 = 0, \qquad \tilde{\rho}_1' = \cos(\theta_S)/4,$$

on $\theta = \pi$. We also assert that the profile must be planar at these very small distances to the contact line for a well-defined microscopic contact angle in the Young equation—requiring $\tilde{\rho}(\tilde{r}, \pi - \theta_S) = 1/2$, at least up to this first-order correction, and leading to

$$\tilde{\rho}_1 = -\frac{\sin\theta_S\cos\theta + \cos\theta_S\sin\theta}{4}, \quad \begin{pmatrix}\tilde{u}_0 \\ \tilde{v}_0\end{pmatrix} = \begin{pmatrix}-\cos\theta \\ \sin\theta\end{pmatrix}.$$

We now consider the stresses and pressure, which in inner variables are scaled with Cn^{-1} (readily seen from eqs. (6)–(7)), as their singular behaviour in the classical model of [13] is the hallmark of the moving contact line problem. The total stress components in polar coordinates and in inner variables are

$$\begin{aligned}\tilde{\mathsf{M}}_{\tilde{r}\tilde{r}} &= \mathrm{Ca}_k{}^{-1}[\{\tilde{\rho}^2(1-\tilde{\rho})^2 + (\partial_\theta\tilde{\rho})^2/\tilde{r}^2 - (\partial_{\tilde{r}}\tilde{\rho})^2\}/2 \\ &\quad + \tilde{\rho}\left\{\partial_{\tilde{r}}^2\tilde{\rho} + \partial_{\tilde{r}}\tilde{\rho}/\tilde{r} + \partial_\theta^2\tilde{\rho}/\tilde{r}^2 - \tilde{\rho}(1-\tilde{\rho})(1-2\tilde{\rho})\right\}] \\ &\quad + \tilde{\rho}\left[4\partial_{\tilde{r}}\tilde{u}/3 - 2\left(\tilde{u} + \partial_\theta\tilde{v}\right)/(3\tilde{r})\right], \\ \tilde{\mathsf{M}}_{\tilde{r}\theta} &= -\mathrm{Ca}_k{}^{-1}\partial_{\tilde{r}}\tilde{\rho}\;\partial_\theta\tilde{\rho}/\tilde{r} + \tilde{\rho}\left[\left(\partial_\theta\tilde{u} - \tilde{v}\right)/\tilde{r} + \partial_{\tilde{r}}\tilde{v}\right], \\ \tilde{\mathsf{M}}_{\theta\theta} &= \mathrm{Ca}_k{}^{-1}[\{\tilde{\rho}^2(1-\tilde{\rho})^2 - (\partial_\theta\tilde{\rho})^2/\tilde{r}^2 + (\partial_{\tilde{r}}\tilde{\rho})^2\}/2 \\ &\quad + \tilde{\rho}\left\{\partial_{\tilde{r}}^2\tilde{\rho} + \partial_{\tilde{r}}\tilde{\rho}/\tilde{r} + \partial_\theta^2\tilde{\rho}/\tilde{r}^2 - \tilde{\rho}(1-\tilde{\rho})(1-2\tilde{\rho})\right\}] \\ &\quad + \tilde{\rho}\left[-2\partial_{\tilde{r}}\tilde{u}/3 + 4\left(\tilde{u} + \partial_\theta\tilde{v}\right)/(3\tilde{r})\right],\end{aligned}$$

so by substituting in our results, we find at leading order $\tilde{\mathsf{M}} = O(1)$, as all $O(1/\tilde{r})$ terms cancel. To obtain the precise form of the stresses, the second-order terms in the governing equations are needed. The pressure in this inner region is given by $\tilde{p} = \tilde{\rho}^2(1-3\tilde{\rho})(1-\tilde{\rho})/(2\,\mathrm{Ca}_k)$, so that as $\tilde{r} \to 0$ it satisfies $\tilde{p} = -1/(32\,\mathrm{Ca}_k) + O(\tilde{r})$, being finite at the contact line. Continuing with these second-order terms, we find the density and velocity corrections

$$\begin{gathered}\tilde{\rho}_2 = C_{\tilde{\rho}_1} + C_{\tilde{\rho}_2}\cos(2\theta), \\ \begin{pmatrix}\tilde{u}_1 \\ \tilde{v}_1\end{pmatrix} = \begin{pmatrix}\sin\theta_S(\cos(2\theta) - 1)/4 - C_{\tilde{v}}\sin(2\theta) \\ -\sin\theta_S\sin(2\theta)/4 + C_{\tilde{v}}(1 - \cos(2\theta))\end{pmatrix},\end{gathered}$$

arising through solving the governing equations

$$\begin{gathered}\tilde{u}_1 = -\sin(\theta_S)/4 - \tilde{v}_1'/2, \quad \tilde{v}_1' = -\tilde{v}_1'''/4, \\ \tilde{\rho}_2' = -\tilde{\rho}_2'''/4,\end{gathered}$$

and boundary conditions

$$\tilde{u}_1 = \tilde{v}_1 = \tilde{\rho}_2' = 0 \qquad \text{on } \theta = \{0, \pi\},$$

at this order, and where the arbitrary constants $C_{\tilde{\rho}_1}$, $C_{\tilde{\rho}_2}$ and $C_{\tilde{v}}$ would be set by the full solution of the inner

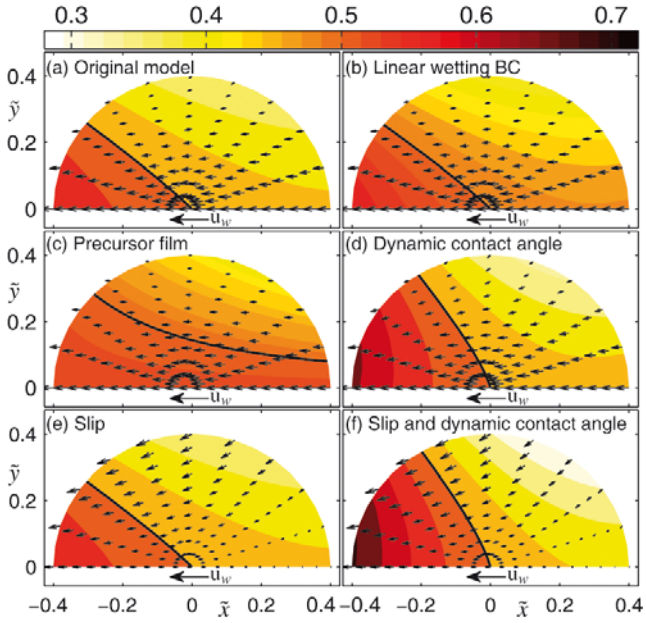

Fig. 3. The asymptotic behaviour of density (contour plots) and velocity (arrows) as the contact line is approached. The driving force in the system is the moving wall.

problem. A possible flow scenario where $C_{\tilde{\rho}_1} = -0.1$, $C_{\tilde{\rho}_2} = 0.3$, $C_{\tilde{v}} = -1$, for $\theta_S = \pi/4$ is shown in fig. 3(a). All of these results allow us to determine the leading-order stress components as

$$\tilde{\mathsf{M}}_{\tilde{r}\tilde{r}} = (M_1 \cos(2\theta) - M_2 \sin(2\theta) + M_3)/32 + O(\tilde{r}),$$
$$\tilde{\mathsf{M}}_{\tilde{r}\tilde{\theta}} = -(M_2 \cos(2\theta) + M_1 \sin(2\theta))/32 + O(\tilde{r}),$$
$$\tilde{\mathsf{M}}_{\tilde{\theta}\tilde{\theta}} = (M_2 \sin(2\theta) - M_1 \cos(2\theta) + M_3)/32 + O(\tilde{r}),$$

where

$$M_1 = \cos(2\theta_S)/\mathrm{Ca}_k + 8\sin\theta_S,$$
$$M_2 = 32C_{\tilde{v}} + \sin(2\theta_S)/\mathrm{Ca}_k,$$
$$M_3 = (1 + 64C_{\tilde{\rho}_1})/\mathrm{Ca}_k - 8\sin\theta_S/3,$$

showing that the stresses are non-singular as $\tilde{r} \to 0$.

3 Extensions

Having demonstrated the ability of our diffuse-interface model to alleviate the moving contact line problem with no-slip applied, we now consider a number of other features of contact line flow. These extensions are to demonstrate the range of boundary conditions derived and applied in the literature, being relevant to various physical situations, and to draw comparisons between diffuse-interface models and one of the more complex continuum theories proposed to deal with contact line flows, the interface formation model of Shikhmurzaev [40].

A recent paper, [19], critically examined this interface formation model of Shikhmurzaev [40]. There, it was shown that the model degenerates to the same macroscopic flow as slip models but it was also seen to have features that most of the simpler models such as Navier-slip do not. In particular, the interface formation model captures finite pressure behaviour, it generalises both the fluid-fluid and the fluid-solid interfaces from their classical models of being sharp and with no-slip respectively through the modelling of surface layers, and the microscopic contact angle is able to vary dynamically from its static value (with its value determined as part of the solution rather than prescribed empirically as it is sometimes for slip models, *e.g.* [41]). Finally, the fluid is able to "roll", as in a moving frame of reference there is no stagnation point at the contact line, allowing particles to reach and transfer through the contact line in finite time. Whilst these features occur at length scales too small to probe with current experimental ability (see discussions in [19]), it is of interest that the diffuse-interface model is capable of similar predictions, with various features added. The model studied thus far already predicts finite pressure at the contact line, and alleviates the stagnation point predicted by slip models through mass transfer. It relaxes the sharp fluid-fluid interface assumption, but has classical no-slip at the wall in contrast to the effective slip of the interface formation model. Although not necessary, this may also be relaxed through carefully prescribing a generalised Navier boundary condition (GNBC), suggesting that the slip velocity is proportional to the total tangential stress (the sum of the viscous and uncompensated Young stress—arising from the deviation of the fluid-fluid interface from its static shape), and derivable using variational arguments from the principle of minimum energy dissipation [42,43]. Our diffuse-interface model also prescribes the microscopic dynamic contact angle θ_d to be equal to the static value θ_S through the wetting boundary condition. An alternative is for this condition to hold at equilibrium, with the density relaxing to it in finite time when out of equilibrium, as initially discussed (but not implemented) for binary fluids [37], and more recently used in numerical simulations [42–45].

For our liquid-gas configuration, the GNBC (of Qian, Wang and Sheng [42,43]) and generalised wetting boundary condition (of the variety of authors mentioned above [37,42–45]) may be considered analogously. In dimensional form the wetting boundary condition is generalised to

$$\alpha\,(\partial_{\bar{t}}\bar{\rho} + \bar{\mathbf{u}}\cdot\boldsymbol{\nabla}\bar{\rho}) = -\bar{L}(\bar{\rho}), \tag{16}$$

where $\bar{L}(\bar{\rho}) = K\mathbf{n}_w\cdot\boldsymbol{\nabla}\bar{\rho} + \bar{f}'_w(\bar{\rho})$, is the wall chemical potential, and $\alpha = 0$ representing instantaneous relaxation to equilibrium. A representative effect of (16) is shown in fig. 3(d), in comparison to (4) in fig. 3(a). The GNBC for this application with inverse slip length $\bar{\beta}$ is then

$$\bar{L}(\bar{\rho})(\mathbf{t}_w\cdot\boldsymbol{\nabla}\bar{\rho}) - \bar{\boldsymbol{\tau}}_{nt} = \bar{\beta}(\bar{\mathbf{u}} - \bar{\mathbf{u}}_w)\cdot\mathbf{t}_w, \tag{17}$$

with $\mathbf{t}_w$ the tangent to the wall, and $\bar{\boldsymbol{\tau}}_{nt}$ the viscous shear stress. Note $\alpha = 0$ reduces to the popular Navier-slip condition. A representative effect of the GNBC from (17) is shown in fig. 3(e), and in combination with (16) in fig. 3(f).

In non-dimensional form in polar coordinates for steady flow in the inner region, (16) reduces to

$$\tilde{L}(\tilde{\rho}) = \mathrm{Ca}_k \, \Pi \, (\tilde{u} \, \partial_{\tilde{r}} \tilde{\rho} + \tilde{v} \, \partial_\theta \tilde{\rho}/\tilde{r}) \,, \tag{18}$$

where $\tilde{L}(\tilde{\rho}) = \pm \partial_\theta \tilde{\rho}/\tilde{r} + \tilde{\rho}(1-\tilde{\rho}) \cos\theta_S$ on $\theta = \{0, \pi\}$, and with another non-dimensional parameter arising, $\Pi = \alpha \rho_L^2/(\mu_L \epsilon)$, describing the extent of the wall relaxation ($\Pi = 0$ being instantaneous). Similarly (17) reduces to

$$\mp \tilde{L}(\tilde{\rho}) \partial_{\tilde{r}} \tilde{\rho} / \mathrm{Ca}_k - \tilde{\rho} \, [(\partial_\theta \tilde{u} - \tilde{v})/\tilde{r} + \partial_{\tilde{r}} \tilde{v}] = \beta (1 \pm \tilde{u}), \tag{19}$$

where $\beta = \bar{\beta}\epsilon/\mu_L$ is the non-dimensional slip parameter, and along with Π are both chosen to be formed with the interface thickness ϵ such that they are considered as $O(1)$ in the limit $\mathrm{Cn} \to 0$.

To consider how (16) allows for microscopic contact angle variation dependent on flow conditions, we note that (16) at equilibrium (denoted with subscript e) gives

$$\bar{L}(\bar{\rho}) = K \mathbf{n}_w \cdot \boldsymbol{\nabla} \bar{\rho}|_e + \bar{f}_w'(\rho_L/2) = 0.$$

Based on calculations in [43,45] for the binary fluid case, we consider a steady, dynamic situation (denoted with subscript d), and see that (16) implies

$$\alpha \, \bar{\mathbf{u}} \cdot \boldsymbol{\nabla} \bar{\rho}|_d = - K \mathbf{n}_w \cdot \boldsymbol{\nabla} \bar{\rho}|_d - \bar{f}_w'(\rho_L/2),$$

thus using the equilibrium result and considering this at the contact line with wall velocity $\bar{\mathbf{u}}_w = -V \mathbf{t}_w$, we find $V\alpha \sin\theta_d = -K(\cos\theta_d - \cos\theta_S)$, or in nondimensional form

$$\mathrm{Ca}_k \, \Pi = (\cos\theta_S - \cos\theta_d)/\sin\theta_d \approx \theta_d - \theta_S,$$

where the final approximation holds for $\theta_d - \theta_S \ll 1$, in agreement with the binary fluid case [45].

Another consideration is the behaviour near the contact line if density gradients near the wall are permitted far from the contact line. Our wall free energy was specifically chosen to prevent this, but we may also consider the two other situations used previously in the literature, namely i) specifying a density at the wall $\bar{\rho} = \rho_a$ on $\partial\Omega$, as in [25], and a representative effect of this shown in fig. 3(c) and ii) choosing a linear form in the density for the wall free energy $\bar{f}_w(\bar{\rho}) = a\bar{\rho}$, as in [26–28,38], and shown in fig. 3(b). To consider the contact line behaviour when i) replaces the wetting boundary condition is straightforward, but for ii), we must understand how to impose the microscopic contact angle to compare to our previous condition. Following [27], we use Young's law $\cos\theta_S = (\sigma_V - \sigma_L)/\sigma$ and compute σ_V and σ_L by integrating the free energy per unit area along the corresponding interface. This gives $\cos\theta_S = [(1-A)^{3/2} - (1+A)^{3/2}]/2$, where $A = 4a\epsilon/(K\rho_L)$ is non-dimensional. This may then be inverted to give the appropriate value of A for a given contact angle θ_S, and corresponds to the non-dimensional boundary condition $\mathrm{Cn} \, \mathbf{n}_w \cdot \boldsymbol{\nabla} \rho = -A/4$.

Adding these features into the diffuse-interface model do not dramatically alter the contact line behaviour, but subtle differences in the asymptotic results are demonstrated, as mentioned, in fig. 3 for selected arbitrary constants, where $\mathrm{Ca}_k = 0.1$ and $\theta_S = \pi/4$, and may be compared to the equilibrium situation in fig. 2. The cases considered are a) the original model (4) without slip or wall relaxation, b) using the linear form for $\bar{f}_w(\bar{\rho})$ in the wetting boundary condition, c) adding a precursor film at the wall (where the wetting boundary condition is replaced by $\rho = \rho_a/\rho_L = 0.53$), d) allowing finite wall relaxation, (18) with $\Pi = 5$, e) including the GNBC ((19) with $\beta = 2$) but with $\Pi = 0$, and f) using (18) with $\Pi = 5$ and (19) with $\beta = 2$. All models behave as expected, resolving the stress and pressure singularities, and including the effects they intend, *e.g.* capturing the film in c), increased microscopic contact angle in d) and f), and reduced wall velocity in e) and f). There are only small differences between cubic and linear wall energy forms near the contact line, mainly that the linear form shows a broader band of density variation. This hints at the important difference that will occur near the wall but far away from the interface, where density gradients will remain present for this linear form.

4 Conclusions

We have shown analytically that a diffuse-interface model is able to resolve the moving contact line problem through relaxing the interface from being sharp to thin, without need to model any further physical effects from the microscale at the contact line. Whilst slip, precursor films and finite-time wall relaxation have been considered, they are *not* necessary to resolve the moving contact line problem. We believe that the present study will motivate further analytical and numerical work with diffuse-interface models, such as to consider heterogeneous walls [46–49]. Of particular interest would also be the inclusion of nonlocal terms into the governing equations; this was considered in [33] for equilibrium wetting using a density-functional theory.

We acknowledge financial support from ERC Advanced Grant No. 247031, and Imperial College through a DTG International Studentship.

References

1. D.L. Hu, B. Chan, J.W.M. Bush, Nature **424**, 663 (2003).
2. Z. Guo, W. Liu, Plant Sci. **172**, 1103 (2007).
3. S.J. Weinstein, K.J. Ruschak, Annu. Rev. Fluid Mech. **36**, 29 (2004).
4. B.-J. deGans, P. Duineveld, U. Schubert, Adv. Mater. **16**, 203 (2004).
5. J.Z. Wang, Z.H. Zheng, H.W. Li, W.T.S. Huck, H. Sirringhaus, Nat. Mater. **3**, 171 (2004).
6. D. Saini, D.N. Rao, SPE Reserv. Eval. Eng. **12**, 702 (2009).
7. E.B. Dussan V., Annu. Rev. Fluid Mech. **11**, 371 (1979).
8. P.G. de Gennes, Rev. Mod. Phys. **57**, 827 (1985).
9. T.D. Blake, J. Colloid Interface Sci. **299**, 1 (2006).

10. D. Bonn, J. Eggers, J. Indekeu, J. Meunier, E. Rolley, Rev. Mod. Phys. **81**, 739 (2009).
11. E.B. Dussan V., S.H. Davis, J. Fluid Mech. **65**, 71 (1974).
12. Y.D. Shikhmurzaev, Physica D **217**, 121 (2006).
13. C. Huh, L.E. Scriven, J. Colloid Interface Sci. **35**, 85 (1971).
14. C.-L. Navier, Mem. Acad. Sci. Inst. Fr. **6**, 389 (1823).
15. M.G. Velarde (Editor), Eur. Phys. J. ST **197**, (2011).
16. L.W. Schwartz, R.R. Eley, J. Colloid Interface Sci. **202**, 173 (1998).
17. D.E. Weidner, L.W. Schwartz, Phys. Fluids **6**, 3535 (1994).
18. Y.D. Shikhmurzaev, Int. J. Multiphase Flow **19**, 589 (1993).
19. D.N. Sibley, N. Savva, S. Kalliadasis, Phys. Fluids **24**, 082105 (2012).
20. M. Renardy, Y. Renardy, J. Li, J. Comput. Phys. **171**, 243 (2001).
21. P. Colinet, A. Rednikov, Eur. Phys. J. ST **197**, 89 (2011).
22. D.M. Anderson, G.B. McFadden, A.A. Wheeler, Annu. Rev. Fluid Mech. **30**, 139 (1998).
23. R. Evans, Adv. Phys. **28**, 143 (1979).
24. P. Yatsyshin, N. Savva, S. Kalliadasis, J. Chem. Phys. **136**, 124113 (2012).
25. L.M. Pismen, Y. Pomeau, Phys. Rev. E **62**, 2480 (2000).
26. P. Seppecher, Int. J. Eng. Sci. **34**, 977 (1996).
27. A.J. Briant, Philos. Trans. Roy. Soc. A **360**, 485 (2002).
28. A.J. Briant, A.J. Wagner, J.M. Yeomans, Phys. Rev. E **69**, 031602 (2004).
29. V.V. Khatavkar, P.D. Anderson, H.E.H. Meijer, J. Fluid Mech. **572**, 367 (2007).
30. H. Ding, P.D.M. Spelt, J. Fluid Mech. **576**, 287 (2007).
31. P. Yue, C. Zhou, J.J. Feng, J. Fluid Mech. **645**, 279 (2010).
32. A. Oron, S.H. Davis, S.G. Bankoff, Rev. Mod. Phys. **69**, 931 (1997).
33. A. Pereira, S. Kalliadasis, J. Fluid Mech. **692**, 53 (2012).
34. A. Hoang, H.P. Kavehpour, Phys. Rev. Lett. **106**, 254501 (2011).
35. L.M. Pismen, Colloids Surf. A **206**, 11 (2002).
36. P. Yue, J.J. Feng, C. Liu, J. Shen, J. Fluid Mech. **515**, 293 (2004).
37. D. Jacqmin, J. Fluid Mech. **402**, 57 (2000).
38. X. Xu, T. Qian, J. Chem. Phys. **133**, 204704 (2010).
39. J.W. Cahn, J.E. Hilliard, J. Chem. Phys. **28**, 258 (1958).
40. Y.D. Shikhmurzaev, *Capillary Flows with Forming Interfaces* (Taylor & Francis, London, 2008).
41. L.M. Hocking, J. Fluid Mech. **211**, 373 (1990).
42. T. Qian, X.-P. Wang, P. Sheng, Phys. Rev. E **68**, 016306 (2003).
43. T. Qian, X.-P. Wang, P. Sheng, J. Fluid Mech. **564**, 333 (2006).
44. P. Yue, J.J. Feng, Eur. Phys. J. ST **197**, 37 (2011).
45. P. Yue, J.J. Feng, Phys. Fluids **23**, 012106 (2011).
46. N. Savva, S. Kalliadasis, Phys. Fluids **21**, 092102 (2009).
47. N. Savva, S. Kalliadasis, G.A. Pavliotis, Phys. Rev. Lett. **104**, 084501 (2010).
48. R. Vellingiri, N. Savva, S. Kalliadasis, Phys. Rev. E **84**, 036305 (2011).
49. C. Wylock, M. Pradas, B. Haut, P. Colinet, S. Kalliadasis, Phys. Fluids **24**, 032108 (2012).